Electronic Supplementary Material (ESI) for Nanoscale.

Supporting Information

Probing Transcription Factor Binding Activity and Downstream Gene Silencing in Living Cells with a DNA Nanoswitch

Alessandro Bertucci, [ab] *Junling Guo,* [a] *Nicolas Oppmann,* [a] *Agata Glab* [a], *Francesco Ricci,* [b] *Frank Caruso,** [a] *and Francesca Cavalieri** [ab]

[a]ARC Centre of Excellence in Convergent Bio-Nano Science and Technology, and the Department of Chemical and Biomolecular Engineering, The University of Melbourne, Parkville, Victoria 3010, Australia
E-mail: francesca.cavalieri@unimelb.edu.au, fcaruso@unimelb.edu.au

[b] Department of Chemistry, University of Rome Tor Vergata, 00133 Rome, Italy

Section S1. DNA Nanoswitch: Design and Binding Properties

The structure of a DNA nanoswitch competent for binding to the transcription factor (TF) NF-κB must include the relevant double-strand binding domain, the most characteristic one being 5′-GGGACTTTC-3′, and its complementary sequence. Using freely available software for analysis of nucleic acids folding (herein, we used mfold,[1] http://unafold.rna.albany.edu/?q=mfold), it is possible to predict with good accuracy DNA conformation thermodynamics, which allows for the design of a DNA construct incorporating the NF-κB binding motif and featuring interconversion between distinct conformations. The sequence for the NF-κB-switch is thus 5′-[Quasar670]-AGTATGGGACTTTCCATACTT[BHQ]-ATTTGAGGAAAGTCCCTCAAAT-3′, where the underlined segment is the NF-κB binding domain, Quasar 670 is the fluorophore conjugated at the 5′-end, and BHQ is Black Hole Quencher introduced as internal modification on thymine 21. This single-strand DNA folds up, giving rise to two definite conformers in thermodynamic equilibrium, as reported in Figure S1.

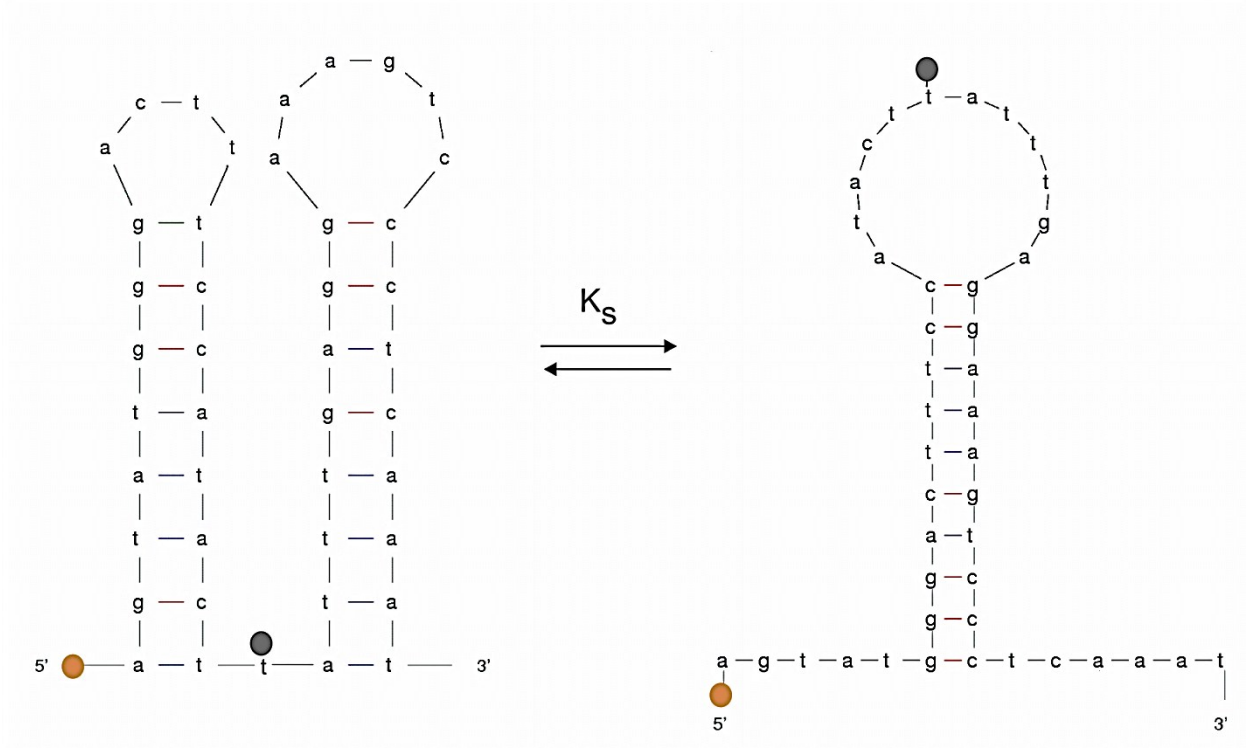

Figure S1. DNA conformations in thermodynamic equilibrium. A DNA nanostructure containing the recognition site for NF-κB is engineered into a molecular switch folded into two conformations in thermodynamic equilibrium. The conformation on the left, the “off-state”, presents the NF-κB binding motif undisclosed and the pair fluorophore–quencher in close proximity (fluorophore depicted as orange circle, quencher as black circle). The conformation on the right, the “binding-competent state” or “on-state”, features the binding domain readily accessible to NF-κB and the fluorophore–quencher couple set apart. Binding of the target TF then shifts the equilibrium towards the “on-state” via a population-shift mechanism (see Figure 1 in the main text).

By using a simulation approach on mfold, it is possible to predict the free energy of the two states in equilibrium, respectively ΔG = −10.55 kcal/mol for the "off-state" and ΔG = −10.47 kcal/mol for the "on-state". Comparison of these values indicates that the "off-state" is thermodynamically more stable than the "on-state" at 37 °C (additionally, a correction of 0.48 kcal/mol has to be taken into account for the free energy value of the "off-state" because of the stacking of the fluorophore and quencher).[2] The conformational free energy parameters allow for the determination of the equilibrium constant K_s (switching constant) with a value of $K_s^{37\ °C}$ = 0.40. As previously demonstrated, a K_s value in the range of 0.2–1 ensures the best trade-off between signal gain (optimal al low K_s) and DNA binding affinity (optimal at high K_s), thus endowing the DNA nanoswitch with the best-performing sensing features. The binding curve for NF-κB and the relative dissociation constant K_d can then be obtained through a titration experiment by monitoring the change in fluorescence intensity of the DNA nanoswitch as the thermodynamic equilibrium shifts towards the "on-state" conformation, driven by binding to NF-κB. For sequential additions of NF-κB in the concentration range of 0.5–250 nM to a solution of 10 nM NF-κB-switch, the binding curve and the corresponding fluorescence emission spectra obtained are as shown in Figure S2.

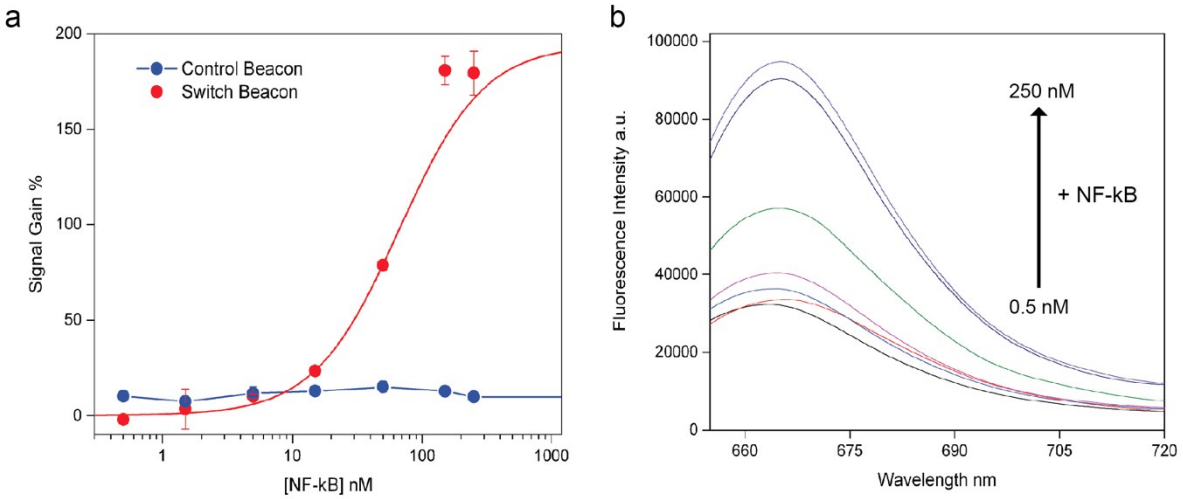

Figure S2. Binding curve of NF-κB and corresponding fluorescence emission evolution. a) Binding curve of the NF-κB-switch (red line) upon binding to its target, reported in terms of fluorescence gain percentage plotted against added concentration of NF-κB (NF-κB-switch 10 nM). A non-NF-κB-binding control sequence (blue line) shows no variations in fluorescence emission for increasing concentrations of NF-κB. b) Evolution of fluorescence emission spectra of the NF-κB-switch at varying concentrations of NF-κB upon titration with NF-κB. The increase in the extent of binding between NF-κB and its target shifts the NF-κB-switch towards the "on-state" conformation, in which the fluorophore Quasar 670 results set apart from the BHQ and its emission is restored.

The above binding curve was obtained by plotting fluorescence intensities expressed as signal gain percentage against concentration of NF-κB. Signal gain values (SG%) are calculated from enhancements in the fluorescence intensity achieved upon addition of NF-κB to an aqueous solution 10 nM NF-κB-switch and expressed as a percentage relative to the initial background fluorescence (intrinsic fluorescence emission of the "off-state"). As only one of the DNA conformers – the "on-state" – can bind to NF-κB, titration data were analyzed according to a Langmuir-type binding process combined with a conformational switch equilibrium, which results in the following equation:

$$SG\% = \frac{m * [NF\kappa B]^n}{K_{app}^{\ n} + [NF\kappa B]^n}$$

where *m* is SG% max, and K_{app} is the apparent dissociation constant and *n* is a coefficient.

K_{app} is defined as follows:

$$K_{app} = K_d^{int}\frac{1 + K_s}{K_s}$$

As reported in the main text, a K_{app} = 66 ± 4 nM was obtained. Accordingly, K_d^{int} , which is the intrinsic dissociation constant of the binding-competent state, is ≈19 nM. Finally, it is noted that the above calculations and values are expressed for NF-κB as dimeric protein. NF-κB is naturally present in the cellular environment and binds to the DNA target region as either p50/p50 homo- or p50/p65 heterodimer.[3]

To have a reliable negative control system, we also designed a DNA nanostructure featuring conformation and background fluorescence compatibility with the NF-κB-switch, yet not displaying any NF-κB binding motif along the strand. Its sequence is 5′-[Quasar670]-AGTATTGTTTTTACAATACTT[BHQ]ATTTGATGTTTTTTCATCAAAT-3′. The fluorescence properties of this DNA construct are reported in Figure 1b in the main text. The structure similarity with the NF-κB-switch ensures comparable behavior with regards to cellular internalization and trafficking.

a

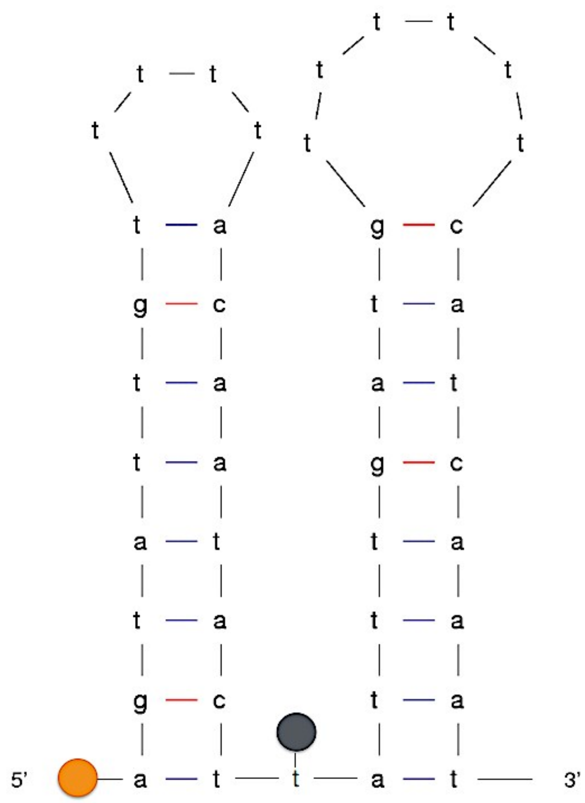

b

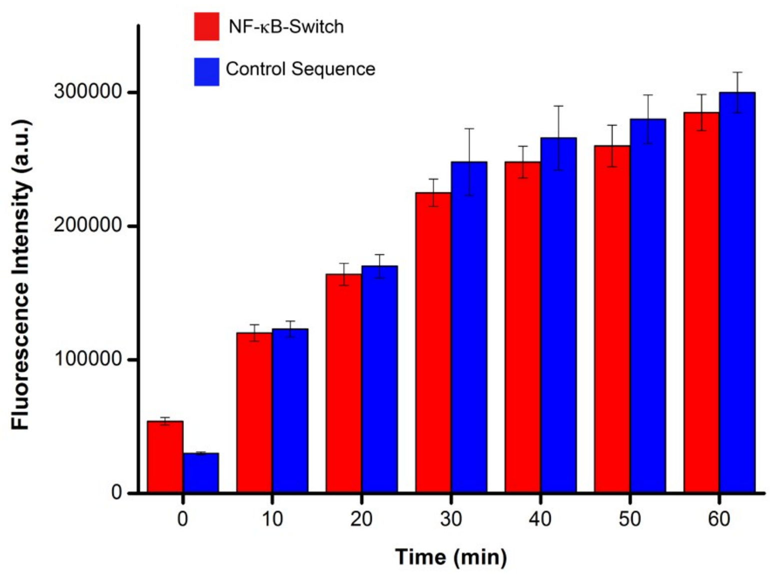

Figure S3. Structural conformation and degradation properties of DNA control sequence. a) This DNA construct features a double stem-loop structure alike the one of the NF-κB-switch, however, lacking the NF-κB binding domain. As no equilibrium between an "off-state" and an "on-state" takes place, no binding-induced events are expected. b) DNase-induced degradation as a function of time of NF-κB-switch and control sequence.

The fluorescence emission spectra of the unwound NF-κB-switch and control sequence (maximum fluorescence intensity) were obtained after hybridization with complementary oligonucleotides in excess (500 nM), respectively 5′-TCAAATAAGTATGGAAAGTCC-3′ for the NF-κB-switch, and 5′-AAAAAACATCAAATAAGTATTGTAAAA-3′ for the control sequence. To verify that the NF-κB-switch and the control sequence undergo the same degradation kinetic we incubated both samples with nuclease. DNase in the concentration of 0.8 UnitsmL^{-1} was added to a solution of 25 nM NF-κB-switch and DNA control sequence, dissolved in DNase buffer at pH 7.4. The corresponding fluorescence emission, resulting from degradation of nucleic acids tagged with Quasar670 and BHQ, was recorded as a function of time as shown in Figure S3b.

Section S2. Gel Electrophoresis

Polyacrylamide gel electrophoresis was used to visualize the formation of the complex between the NF-κB-switch and NF-κB. A native gel without denaturing agents was prepared to maintain the TF in its active state to bind to the target DNA domain. The prepared gel had a final concentration of 12% acrylamide/bis-acrylamide (29:1 (w/w)) in 1× TBE-Buffer and was run in 0.5× TBE-Buffer at 180 V for 25 min. After separation, staining with SYBR® Gold for the visualization of the DNA and with Invitrogen Simply-Blue Stain for visualization of the protein was carried out. Preparation of the test sample, containing the NF-κB/NF-κB-switch complex, or the corresponding negative control, was done by mixing the TF with either NF-κB-switch or the negative control, respectively, and incubating for 15 min at 37 °C. The final concentration of the reactants was 2.04 μM for the NF-κB and 0.1 μM for the DNA nanoconstructs. After DNA staining, it was possible to spot a distinct band on top of lane 2, which was instead missing in lanes 3 and 4.

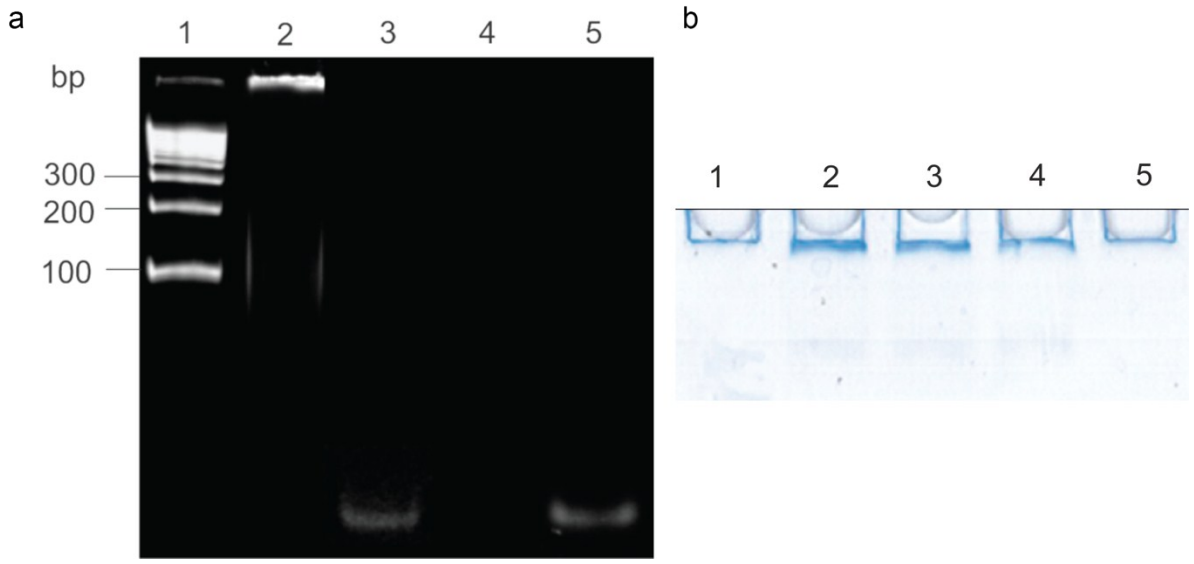

Figure S4. a) Polyacrylamide gel after staining with SYBR® Gold. The gel was loaded as such: lane 2, NF-κB/NF-κB-switch complex; lane 3, NF-κB + negative control DNA sequence; lane 4, pure NF-κB; and lane 5, NF-κB-switch only. b) Polyacrylamide gel after staining with Invitrogen Simply-Blue Stain for protein detection. After DNA staining, the gel was counter-stained with coomassie blue for the visualization of NF-κB, which resulted in blue bands at the top of lanes 2–4, indicating that NF-κB does not run down the lane.

Section S3. Cell Viability Assay

Cell viability under the experimental conditions used for cell transfection and incubation with the DNA nanoswitch was investigated. MTT assay for cell viability was carried out for different cell samples: (1) cells cultured in the absence of any transfection (control untreated), (2) cells transfected with the control DNA sequence (Control DNA sequence), (3) cells transfected with the NF-κB-switch (NF-κB-switch), and (4) cells treated with 30% dimethyl sulfoxide (30% DMSO). PC3 cells, approximately 8,000, were seeded in 96-well culture plates, followed by addition of 0.1 mL culture medium and incubation overnight. Transfection with the NF-κB-switch or the control sequence was then performed using lipofectamine as per the transfection protocol provided by the supplier so that the final concentration of the DNA nanoswitch in each well was 25 nM. After incubation for 4 h at 37 °C in 5% CO_2, the transfection medium was discarded and replaced with fresh culture medium, followed by incubation for the next 24 h. In parallel, cell samples in the absence of treatment (negative control) or incubated with 30% DMSO (positive control) were cultured. The MTT assay was then performed according to standard protocols, and the cell samples were analyzed using a plate reader. Six independent replicates were obtained for each treatment. The results are reported in Figure S9 in the form of a histogram, which shows no difference in cell viability between the untreated populations of cells and the ones that were administered the DNA-lipoplex formulations (both NF-κB-switch and control sequence). This set of data shows that under the experimental conditions used throughout this study: (1) lipofectamine formulation does not induce cytotoxic effects, as demonstrated by the control sequence treatment that exerts no biological activity or targeting; and (2) the NF-κB-switch formulation does not trigger any toxic effect compared to the untreated samples – it is important to demonstrate that the standard metabolism of the treated PC3 cells does not undergo any substantial variation, showing that NF-κB imaging and sensing is representative of cells under normal metabolic conditions. We ascribe these findings to the fact that the final intracellular concentration of the active NF-κB-switch after transfection and endosomal escape, a process that, for lipid nanoparticle-mediated siRNA delivery, is reported to be no more efficient than 1–2%[7] is low enough not to induce any significant interference to the cellular metabolism. Affinity competition for NF-κB between the DNA nanoswitch and the natural binding site located on genomic DNA might also take place. This may prompt the two respective NF-κB/DNA complexes to undergo a dynamic equilibrium, which ultimately prevents poisonous sequestering of available active TF. We eventually envision that higher transfection doses and different experimental conditions might be investigated to study potential therapeutic actions and TF-targeting-mediated biological interference.

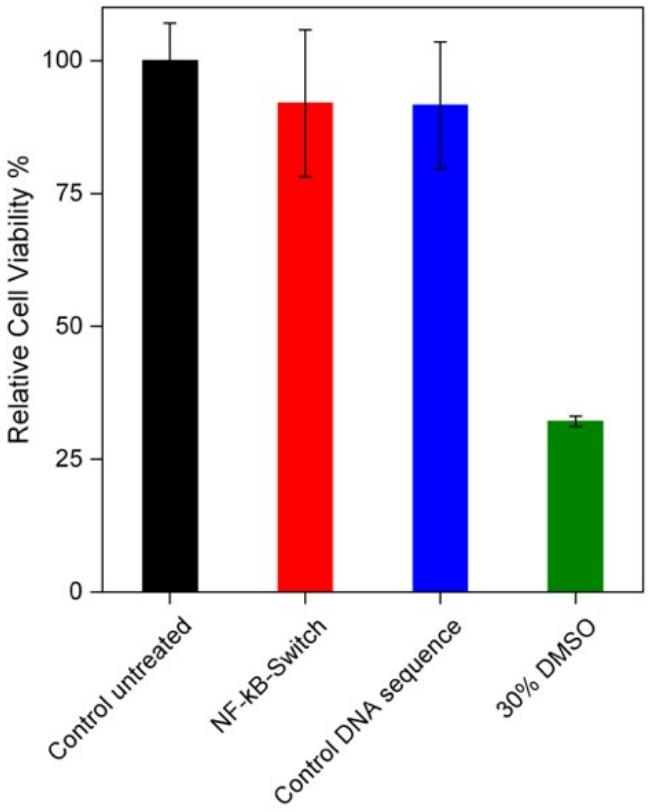

Figure S5. MTT assay for cell viability. The histogram reports the relative cell viability measured by MTT assay for differently treated cell samples. No changes in cell viability compared to the untreated cells (black bar) are observed for cells administered with the NF-κB-switch (25 nM, Lipofectamine as carrier, red bar) or control DNA sequence (25 nM, lipofectamine as carrier, blue bar). A drastic toxic effect is obtained when cells are incubated with 30% DMSO as positive control (green bar). The histogram displays the mean values of six independent sample measurements obtained under each studied condition and error bars denote the standard deviation.

Section S4. NF-κB Imaging on Fixed Cells

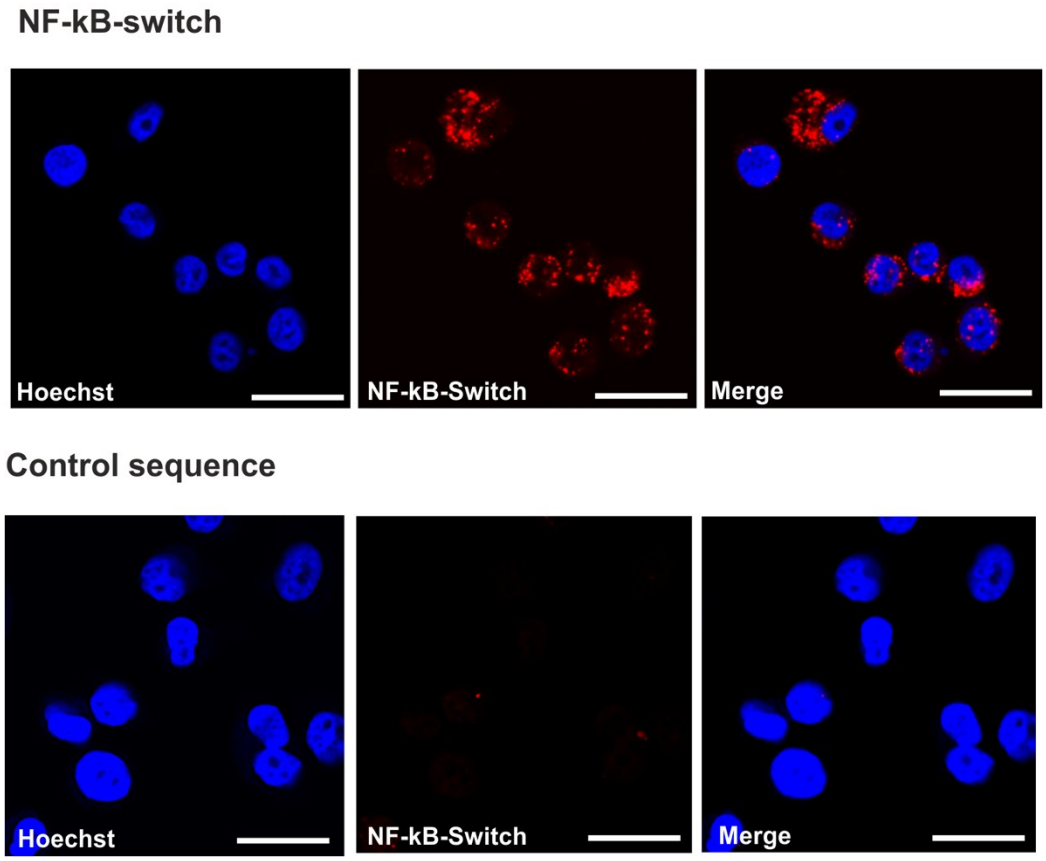

Figure S6. Confocal micrographs of PC3 cells transfected with 25 nM NF-κB-switch (upper panels) or control sequence (bottom panels) for 4 h and subsequently cultured for 24 h. Cell were then fixed and analyzed by confocal laser scanning microscopy. The cell nuclei are stained in blue with Hoechst 33342. When the NF-κB-switch is used, a bright intracellular red emission can be observed (Quasar 670), which is due to the binding-responsive switching of the DNA probe to the "on-state". Cells treated with the control sequence do not show any intracellular fluorescence emission. Scale bars are 50 μm.

Section S5. Intracellular Uptake of DNA Nanoswitch

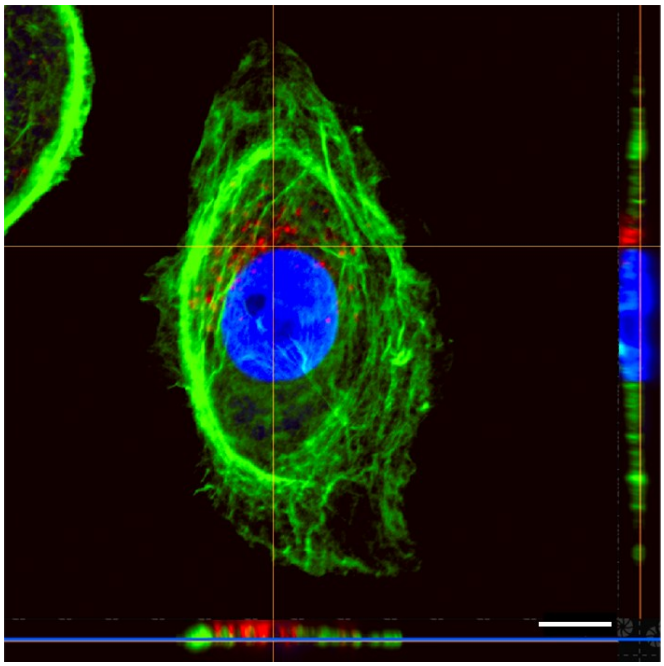

Figure S7. Confocal *Z*-stack of internalized NF-κB-switch. Orthogonal view of a PC3 cell and emitting NF-κB-switch taken by *Z*-stack acquisition reveal the localization of the DNA nanoswitch inside the cell. This in turn confirms the occurrence of cellular uptake and intracellular bio-trafficking. The cell nucleus is stained with Hoechst 33342 (blue signal) and actin filaments are stained with Alexa Fluor 488 Phalloidin (green signal). The red emission (Quasar 670) comes from the NF-κB-switch. NF-κB-switch transfection and incubation were performed as described in the *Experimental Section*; Phalloidin and Hoechst staining were applied after cell fixation. Scale bar is 15 μm.

Section S6. On-Target Localization of NF-κB-Switch

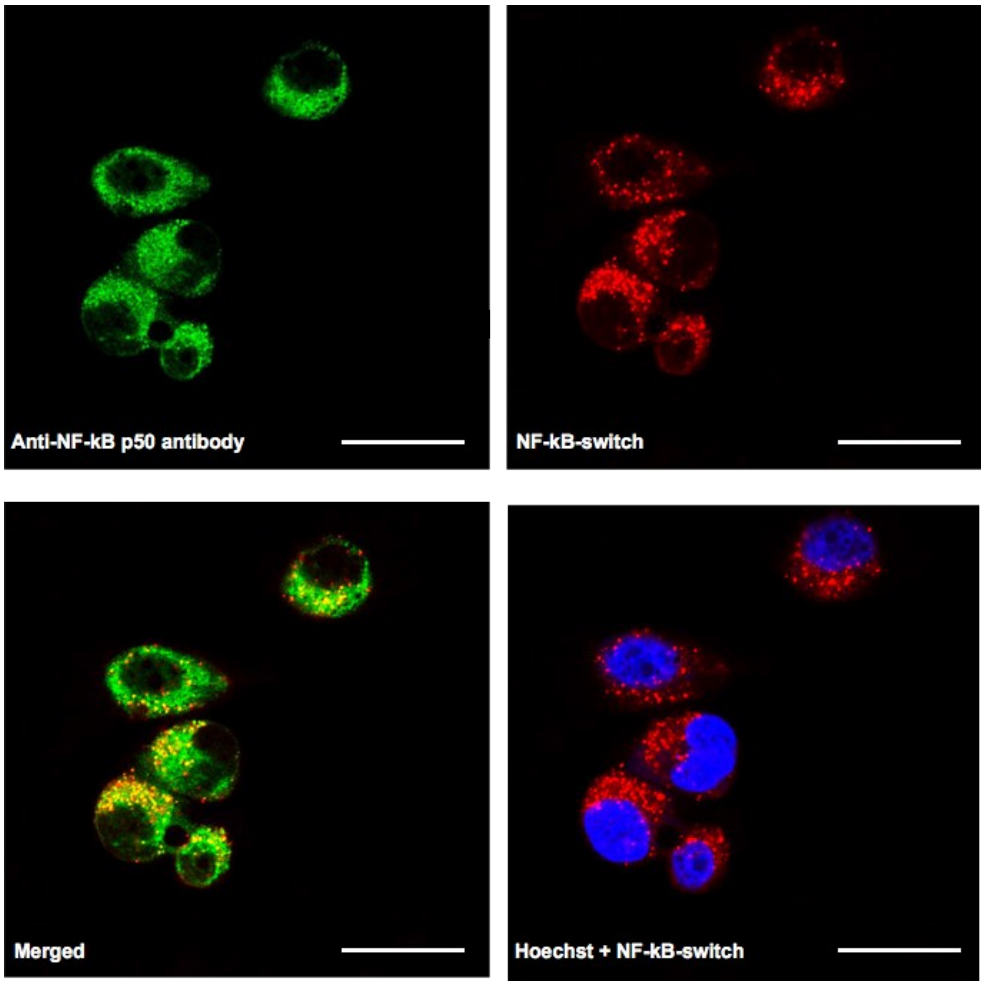

Figure S8. Co-localization of NF-κB-switch and antibody staining. Confocal micrographs show the distribution of the NF-κB-switch (red signal) is co-localized with that of anti-NF-κB p50 antibody, Alexa Fluor 488, (green signal) used to co-stain NF-κB after cell fixation. NF-κB-switch transfection, incubation, and antibody staining were performed as described in the *Experimental Section*. Scale bar is 50 μm.

Section S7. STORM Imaging

Stochastic optical reconstruction microscopy (STORM) is based on the detection and localization of single fluorescent molecules. Imaging is achieved by using photo-switchable probes that can be transferred to a reversible non-fluorescent OFF state (dark excited state) upon irradiation with light of appropriate wavelength and intensity. Either spontaneously or photo-induced upon irradiation with a second laser, a sparse subset of fluorophores is stochastically re-activated (blinking) and imaged over many cycles. As the density of the activated fluorophores is very low, the blinking molecules can be readily separated from one another, and each individual fluorophore can be localized with high accuracy beyond the diffraction-limited resolution. Iterating this procedure over multiple cycles of activation allows for the reconstruction of a super-resolved STORM image.[4] Cyanine dyes and structurally similar molecules have emerged as one of the best-performing class of STORM fluorophores in light of their reversible photoswitching mechanism.[5] As two specific fluorophores can work in concert as an activator–reporter pair, the development of photo-switchable probes with distinct colors (e.g., different activators coupled to the same reporter) has paved the way to multi-channel (multi-color) STORM acquisition.[6] This naturally allows for super-resolved co-localization analysis upon choice of complementary combinations of activator–reporter probes.

In this study, we followed the cellular internalization pathway of the DNA nanoswitch using a NF-κB-switch labelled with the couple Quasar 570–Quasar 670, namely 5′-[Quasar670]-AGTATGGGACTTTCCATACTT[Quasar570]-ATTTGAGGAAAGTCCCTCAAAT-3′. This allows for harnessing the activation of Quasar 570 and selectively acquiring the blinking emission of the reporter Quasar 670 through the paired channel 561–647 nm. To orthogonally visualize cellular vesicles of interest, we prepared specific antibodies dual-labelled with a complementary activator–reporter couple, Alexa Fluor 488 as activator and Alexa Fluor 647 as reporter. This pair enables selective acquisition through the paired channel 488–647 nm. Hence, dual-labelled secondary antibodies were prepared as reported in the *Experimental Section* to allow for staining of early endosome and late endosome/lysosome structures. 2D STORM multi-color acquisition was achieved with imaging cycles containing one frame of activation laser illumination (488 nm or 561 nm) followed by three frames of imaging laser illumination (647 nm) at 28 frames per second. The power of the activation lasers was typically 1% and that of the imaging laser was 100%. As the red imaging laser itself can activate the dark-state A647 in an activator-independent manner, we used an image analysis algorithm to evaluate and subtract the non-specific activation contribution in any local region of the sample and the cross-talk between color channels. The cross-talk mainly comes from the small cross activation of AF647 by the AF488-AF555.

Section S8. Detection of siRNA-Mediated Silencing of NF-κB Expression Using Combined Immunostaining–Flow Cytometry

To confirm the effect of the siRNA-mediated silencing of NF-κB, we performed the same RNAi experiment as described in the *Experimental Section* but used an antibody-based labeling approach to analyze samples by flow cytometry. This is also important for validating, through an independent technique, the results obtained for the real-time monitoring of the magnitude of the siRNA treatment using the NF-κB-switch as sensing probe. To do so, PC3 cells, approximately 50,000, were seeded in 24-well culture plates, followed by addition of 0.5 mL culture medium and incubation overnight. Transfection with the siRNA formulation (against NF-κB, and against Luciferase as additional control – refer to the *Experimental Section*) was carried out using lipofectamine as per the transfection protocol provided by the supplier so that the final concentration of siRNA in each well was either 50 nM or 200 nM (0.5 mL serum-free medium Opti-MEM, 30% DNA-lipoplex solution). After incubation for 4 h at 37 °C in 5% CO_2, the transfection medium was discarded and replaced with fresh complete culture medium, followed by incubation for the next 48 h. Finally, cells were harvested using an enzyme-free cell dissociation buffer, washed with PBS (3×), fixed, permeabilized, and blocked under standard conditions (see *Experimental Section*), and intracellular NF-κB was immunostained by using a primary anti-NF-κB p50 antibody, Alexa Fluor 488 conjugated (2.5 μg/mL, 1 h, 25 °C). Cells were finally washed with PBS (3×) and analyzed via flow cytometry by means of an Apogee Flow System. Green 488 fluorescence channel was used to detect the intracellular emission of the NF-κB-switch. Data were collected through the dedicated Apogee software and further processed with FlowJo™. All experiments were reproduced in triplicate and statistical analysis was carried out using OriginPro (OriginLab™). The results are reported in Figure S8, which shows consistencies with the outputs registered for the NF-κB-switch-based siRNA experiment in the main text (Figure 6).

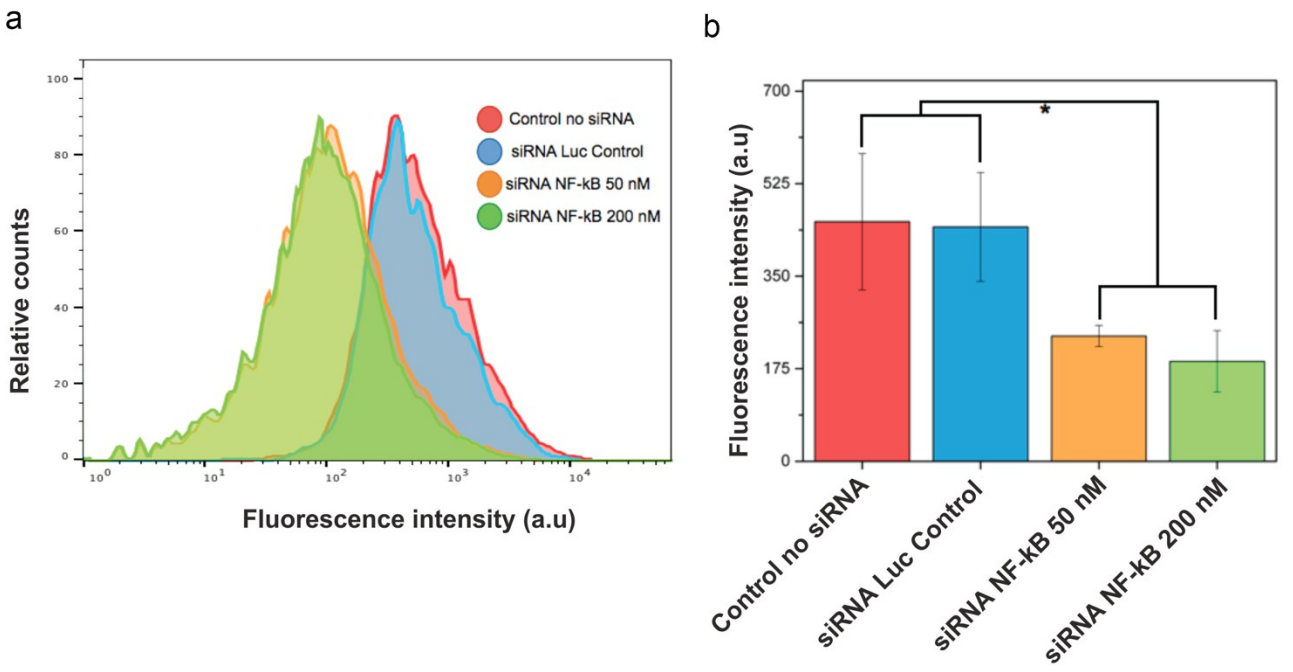

Figure S9. SiRNA-mediated silencing of NF-κB and combined immunostaining–flow cytometry analysis. a) Flow cytometry profiles of PC3 cells treated with different siRNA formulations and immunostained after fixation for NF-κB. Representative profiles are reported for cells in the absence of treatment (Control no siRNA, red line), for cells administered with a 200 nM dose of control siRNA against Luciferase (siRNA Luc Control, blue line), and for cells transfected with doses of respectively 50 nM (siRNA NF-κB 50 nM, orange line) and 200 nm (siRNA NF-κB 200 nM, green line) of siRNA formulation against NF-κB. b) Histogram reporting the mean values of fluorescence intensity collected for the above samples. Experiments are reproduced in triplicate, error bars denote standard deviations, and statistically significant difference is reported as * $p < 0.005$.

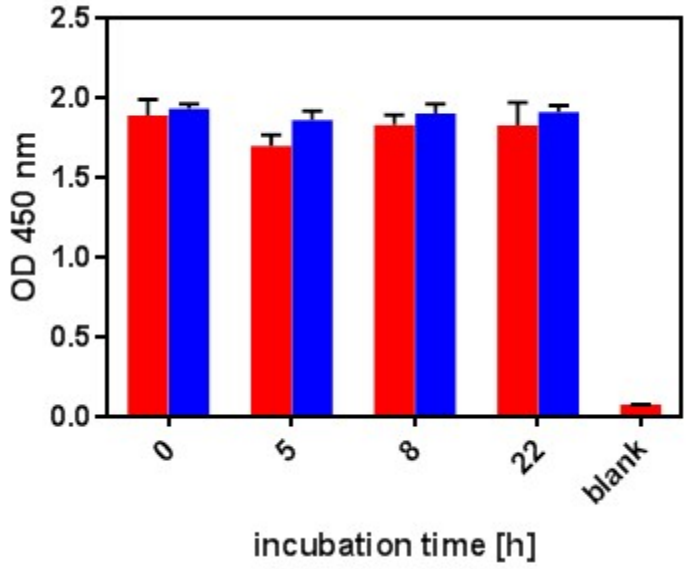

Figure S10. **PC3 cell extracts analysis for total NF-kB.** Red bars indicate transfected cells at different time points (0, 5, 8, 22 h) after transfection. Blue bars show the samples of non- transfected cells incubated for the same amount of hours. Data from triplicate measurements (mean +/- SD) are plotted and compared to 1x Cell Extraction Buffer (blank).

References

[1] M. Zuker, *Nucleic Acids Res.* **2003**, *31*, 3406.
[2] A. Vallée-Bélisle, A. J. Bonham, N. O. Reich, F. Ricci, K. W. Plaxco, *J. Am. Chem. Soc.* **2011**, *133*, 13836-13839.
[3] M. Karin, Y. Cao, F. R. Greten, Z. W. Li, *Nat. Rev. Cancer* **2002**, *2*, 301.
[4] X. Zhuang, *Nat. Photonics* **2009**, *3*, 365.
[5] G. T. Dempsey, M. Bates, W. E. Kowtoniuk, D. R. Liu, R. Y. Tsien, X. Zhuang, *J. Am. Chem. Soc.* **2009**, *131*, 18192.
[6] M. Bates, B. Huang, G. T. Dempsey, X. Zhuang, *Science* **2007**, *317*, 1749.
[7] J. Gilleron, W. Querbes, A. Zeigerer, A. Borodovsky, G. Marsico, U. Schubert, K. Manygoats, S. Seifert, C. Andree, M. Stoter, H. Epstein-Barash, L. Zhang, V. Koteliansky, K. Fitzgerald, E. Fava, M. Bickle, Y. Kalaidzidis, A. Akinc, M. Maier, M. Zerial, *Nat. Biotechnol.* **2013**, *31*, 638.